THE MAGNETIC STRUCTURE AND GENERATION OF EUV FLARE RIBBONS

L. FLETCHER[1] and H. HUDSON[2]
[1]*Department of Physics and Astronomy, Glasgow University, Glasgow G12 8QQ, Scotland, U.K.*
(e-mail: lyndsay@astro.gla.ac.uk)
[2]*SPRC/ISAS, 3-1-1 Yoshinodai, Sagamihara, Kanagawa 229, Japan*
(e-mail: hudson@isass0.solar.isas.ac.jp)

(Accepted 3 August 2001)

Abstract. The 'ribbons' of two-ribbon flares show complicated patterns reflecting the linkages of coronal magnetic field lines through the lower solar atmosphere. We describe the morphology of the EUV ribbons of the July 14, 2000 flare, as seen in SOHO, TRACE, and *Yohkoh* data, from this point of view. A successful co-alignment of the TRACE, SOHO/MDI and *Yohkoh*/HXT data has allowed us to locate the EUV ribbon positions on the underlying field to within $\sim 2''$, and thus to investigate the relationship between the ribbons and the field, and also the sites of electron precipitation. We have also made a determination of the longitudinal magnetic flux involved in the flare reconnection event, an important parameter in flare energetic considerations. There are several respects in which the observations differ from what would be expected in the commonly-adopted models for flares. Firstly, the flare ribbons differ in fine structure from the (line-of-sight) magnetic field patterns underlying them, apparently propagating through regions of very weak and probably mixed polarity. Secondly, the ribbons split or bifurcate. Thirdly, the amount of line-of-sight flux passed over by the ribbons in the negative and positive fields is not equal. Fourthly, the strongest hard X-ray sources are observed to originate in stronger field regions. Based on a comparison between HXT and EUV time-profiles we suggest that emission in the EUV ribbons is caused by electron bombardment of the lower atmosphere, supporting the hypothesis that flare ribbons map out the chromospheric footpoints of magnetic field lines newly linked by reconnection. We describe the interpretation of our observations within the standard model, and the implications for the distribution of magnetic fields in this active region.

1. Introduction

Solar flares often exhibit a two-ribbon structure in the chromosphere (e.g., in Hα), and this pattern becomes especially pronounced for long-duration events of the type often associated with coronal mass ejections. The two-ribbon flare, as seen in Hα, has long been an object of study via ground-based observations (e.g., Švestka, 1976). This structure, together with the observation of loop prominence systems ('post-flare loops' or 'sporadic coronal condensations' in early literature) led to the first ideas regarding coronal energy storage and flare development (Bruzek 1964). Above the ribbons, and bridging the magnetic inversion line in the photosphere, this picture envisions arcades of magnetic loops filled with hot plasma and visible in soft X-rays. For an eruptive flare or a CME, open field lines merge and reconnect

Solar Physics **204:** 71–91, 2001.

at higher and higher altitudes in the corona (Kopp and Pneuman, 1976). Thermal conduction from these loops, or particle bombardment from the reconnection site, then provides the energy source for the ribbon emissions at chromospheric and transition-region wavelengths. The result of this rising reconnection region, connecting pairs of fieldlines at greater and greater distances, is that the ribbons of footpoints move apart. This can be seen in EUV observations such as those reported here, as well as in Hα.

This model makes several simple predictions which can be qualitatively and quantitatively tested with our dataset. Firstly, because every negative footpoint has its positive counterpart, in principle one flare ribbon should be entirely within negative field regions, and the other entirely within positive field regions. Furthermore, the total negative magnetic flux swept across by one ribbon in a given time should be equal in magnitude to that swept out by the ribbon in the positive field.

We also address the nature of the UV and EUV ribbons, examining whether they are consistent with being excited by direct bombardment by particles accelerated in the solar flare, or with being the conductively heated, high density ends of overlying hot flare loops. This question relates closely to the discussion of whether chromospheric evaporation – the inferred upwards expansion of the chromosphere – in two-ribbon flares is driven by beam heating or by conduction. Following reconnection, energy to drive evaporation can reach the chromosphere by two main channels. If the newly-reconnected magnetic flux tube undergoes heating, such that there is a strong temperature gradient established between corona and chromosphere, chromospheric heating and evaporation is driven by conduction (this is normally characterised as 'gentle' evaporation). However, if loop heating is not strong, but a large quantity of particles is accelerated, then the chromosphere is energised by direct particle bombardment, which can heat the atmosphere quickly and give rise to rapid, explosive evaporation.

There are observational arguments for both mechanisms. Masuda, Kosugi, and Hudson (2001) have shown that ribbon geometry also appears in hard X-rays (HXRs), suggesting an important energetic role played by electrons. However, Czaykowska *et al.* (1999) using the SOHO Coronal Diagnostic Spectrometer have directly observed the evaporative flow from the chromospheric ribbons into the corona, without HXRs. They calculate that for the observed upflow speeds, observable HXR emission should result, and argue that its absence suggests either conductively-driven evaporation, or possibly protons as a driver (Czaykowska, Alexander and De Pontieu, 2001). It is also possible, of course, that the different mechanisms implied reflect different phases of the flare.

Conductive heating from overlying hot loops is the favoured mechanism for 'moss', the patches of highly structured, dynamic, bright, low-lying EUV emission seen underlying X-ray loops in active regions (Berger *et al.*, 1999; Fletcher and De Pontieu, 1999). The name 'moss' describes the 'texture' of the emission in TRACE EUV images. Flare ribbons, which appear in some events as 'moving moss' in the TRACE 171 Å channel, are also formed low in the atmosphere. The question of

their formation is, in some ways, similar to that of moss. Like moss, they appear only by virtue of a large-scale coronal energy input, so the corona determines their global distribution, but in their evolution and fine detail they must be influenced by the small-scale photospheric fields.

In this paper we describe flare ribbons as seen in EUV and hard X-ray (HXR) images (TRACE and *Yohkoh* HXT), using the 'Bastille Day 2000' X-class flare as an excellent example. We overlay these transition-region ribbons on line-of-sight magnetograms from the Michelson Doppler Imager (MDI; Scherrer *et al.*, 1995) on board the Solar and Heliospheric Observatory (SOHO; Domingo, Fleck, and Poland, 1995). In Section 2 we describe the flare event and the overall ribbon behaviour, and in Sections 2.2 and 2.3 we study the relationship between ribbons and field. The relative evolution of HXR and EUV sources is studied in Section 3, and discussion and conclusions presented in Section 4.

2. The 'Bastille Day 2000' Flare

This flare was one of the more energetic events (X5.7, 2B) of the current solar maximum, and was extremely well observed by EUV, X-ray, and particle detectors. It involved filament eruption, in two stages, from a large active region, and resulted in a beautifully cylindrical arcade structure extending across more than 10^{10} cm (0.2 $R_\odot$). It occurred near disk centre (N17 E01, in NOAA active region 9077) and involved an extremely regular EUV and X-ray arcade that developed in major steps following the filament eruptions. The peak 15 400 MHz radio flux of 5500 s.f.u. marked it as a major impulsive event, involving strong magnetic fields. It also exhibited the behavior of a long-decay event (LDE), consistent with the formation of the coronal arcade structure.

2.1. Overall evolution of ribbons and loops in the east

Following the first stage of the flare – the eruption in the western part of the active region (between 10:04 UT and 10:23 UT in TRACE UV) bright post-flare loops are visible stretching from $\sim x = 0''$ to $x = 100''$, joining two sets of footpoints which form and spread between 10:08 UT and 10:30 UT. This first eruption also affects the eastern part of the active region, in that a *single* ribbon of stationary EUV emission – apparently footpoint emission – is also visible in the east, suggesting magnetic connections between the east and west parts of the flare. In this paper, we concentrate on the second part of the flare, which led to the formation of flare ribbons and post-flare loops in the eastern part of the region. Figures 1 and 2 show some key times in the evolution of the ribbons.

At 10:17 UT, although there is as yet no sign of an eruption in the eastern part, the single ribbon of bright EUV sources mentioned above is already visible, but stationary, in negative polarity plage, to the south of the neutral line. Wispy

material is ejected between 10:19 and 10:30 UT – clearly visible in TRACE 1600 Å images. However, not until 10:24 UT do we begin to see (a) movement of this southern ribbon or (b) clear evidence in either UV or EUV of a counterpart ribbon in positive field to the north of the neutral line. The counterpart ribbon forms in stages; between 10:24 and 10:27 UT it extends eastwards, eventually stretching between $x = (-40'', 0'')$, or approximately half of the final length of the ribbon. At 10:27:22 footpoints in the second half become visible, and brighten until at around 10:29 UT the complete northern ribbon is seen in both EUV and UV wavelengths.

Between 10:20 UT and 10:25 UT there are a number of small HXR bursts, but the large HXR burst corresponding to this part of the flare occurs between 10:25 UT and 10:28 UT, with a HXR peak (in the HXT M2 channel, which is assumed to be dominated by non-thermal electron-proton bremsstrahlung) at 10:27 UT (see Figure 7). Shortly after the large HXR burst, the northern ribbon completes.

Between 10:24 UT and 10:29 UT the two ribbons move apart; at EUV wavelengths the ribbons remain single narrow structures but in the UV the ribbons broaden, and appear to bifurcate, with one branch having the position of the ribbon before spreading started, and the other branch moving outwards from it, following the EUV ribbon positions.

Post-flare loops at TRACE 1600 Å temperatures become visible in this part of the active region between 10:36:52 UT and 10:38:40 UT, and last until at least 10:48 UT. In TRACE EUV wavelengths, post-flare loops become visible from about 10:26 UT onwards.

2.2. The underlying magnetic field

It is to be presumed that the formation and propagation of flare ribbons is influenced not only by the energisation process in the flare, but also by the coronal and chromospheric magnetic field distributions. Taken overall, the location and evolution of the ribbons is what one would expect in the context of the standard flare model – i.e., spreading ribbons, one on either side of the neutral line. But we wish to examine the relationship between ribbon and field in more detail. To this end, we must accurately coalign the TRACE data with simultaneous magnetic field data. We use magnetograms from the Michelson Doppler Imager instrument on the SOHO satellite, which are taken at 96 minute intervals, with a pixel size of $1.98''$. The nearest magnetograms are at 09:36 UT and 11:12 UT.

Coalignment is in principle possible using the pointing information of the two instruments, but in practice it is known that there are (as yet) unquantified errors in the TRACE pointing, which can be on the order of $10''$. We hope to look at the relationship between ribbons and field on a smaller scale than this, and have therefore determined the coalignment of data from the two instruments via cross-correlation of images made in the white-light channel of TRACE, and the MDI continuum images. We clip areas from a TRACE white-light (WL) image and an MDI continuum image made at approximately the same time which contain the

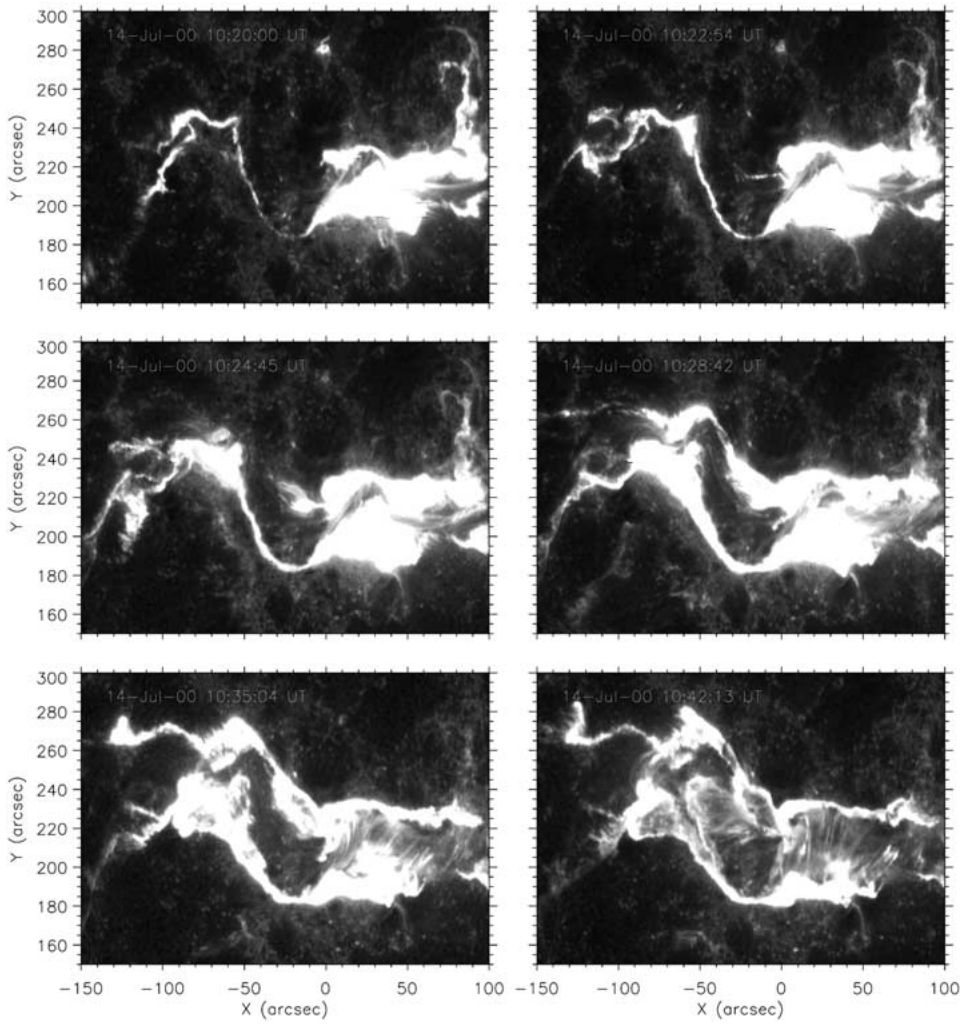

Figure 1. The evolution of the flare ribbons as seen in the TRACE 1600 Å channel between 10:19 UT and 10:42 UT; we are concerned with the eastern half of the region, from $x = -150''$ to $x = 0''$. Note that early in the event, only the southern ribbon in the eastern half is visible. The northern half is complete at 10:28:42 UT. In UV the ribbons show a tendency to thicken and 'bifurcate' as is seen in the bottom two panels.

active region, and which have identical co-ordinate values for the corner pixels, in the pointing system defined for each instrument. (If the pointing were identical between the two, and taking into account solar rotation, these two areas would be identical; they are not – one is clearly offset from the other.) We then rebin the TRACE image to the same pixel size as the MDI image, and cross-correlate the two images. This procedure returns a value of the offset between the TRACE WL and MDI continuum images (which includes the pointing offset and rotation).

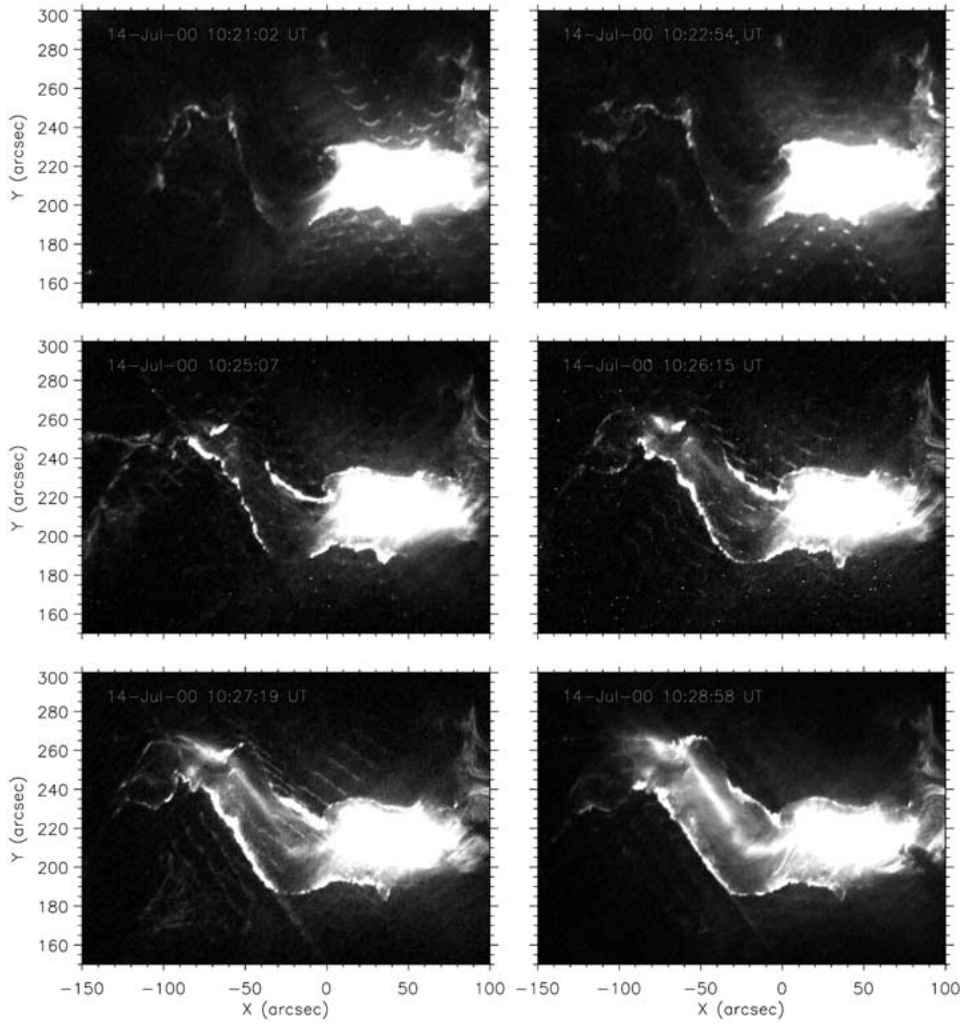

Figure 2. The evolution of the flare ribbons as seen in the TRACE 195 Å channel between 10:20 UT and 10:30 UT. Again this shows that in the initial stages of the flare in the eastern part of the structure, only the southern ribbon is visible; it is practically complete in EUV at 10:28:53 UT, and post-flare loops are clearly visible

Repeating this for each TRACE WL image made during the period of the flare gives a vector of offsets through time. An example of an overlay of MDI continuum on TRACE WL, following this cross-correlation, is shown in Figure 3. We expect that the correlation is good to ~ 1 MDI pixel in each direction, i.e., $\pm 2''$.

It is known also that the TRACE EUV channel pointing is offset with respect to the TRACE WL channel, due to the different focus positions of the two. When overlaying TRACE EUV with MDI, this additional correction must be applied.

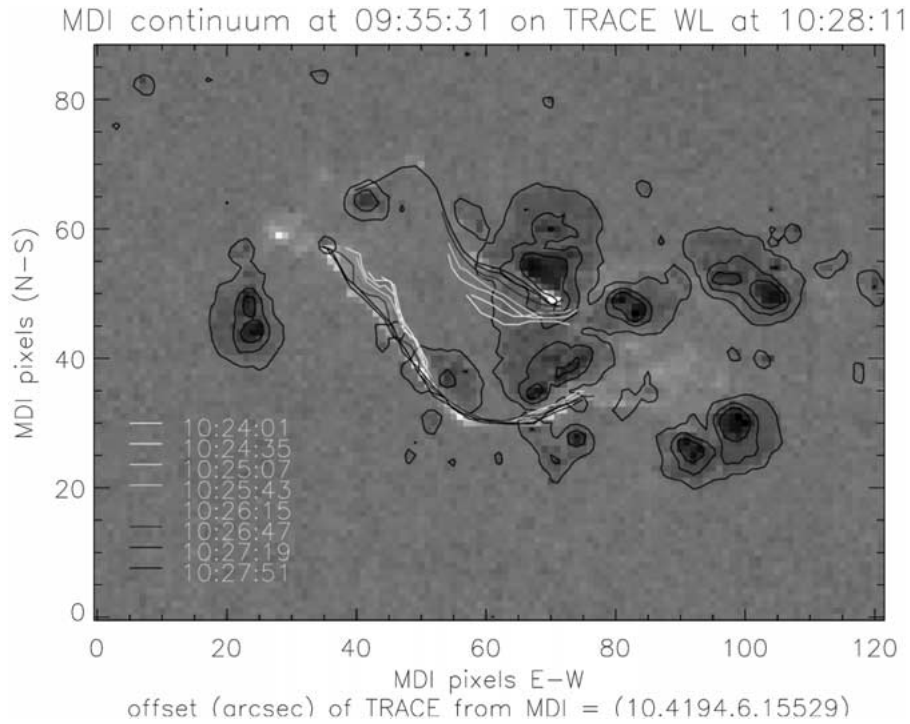

Figure 3. MDI continuum (*contours*) on TRACE WL following rebinning of the TRACE image and cross-correlation. Note, most of the E–W offset is due to rotation, but the N–S offset is pointing drift. The ribbons form in the left-hand part of the image, from the major sunspot east. The locations of the outer edges of the spreading EUV ribbons are also shown superimposed.

Having done this, we are in a position to overlay on the field the locations of the outer edges of the TRACE EUV ribbons as a function of time as they separate. We define the ribbon location by pointing and clicking on an image at several points (~ 15 typically) along the ribbon, converting these locations to heliographic co-ordinates in the TRACE 195 Å coordinate system, and then applying the offset correction nearest in time to the time at which the TRACE image was made. The footpoint positions can then be overlaid on an MDI magnetogram. The result of this procedure is seen in Figure 4.

Figure 4 exhibits a few curious features. First of all, the eastern half of the northern ribbon is not in strong positive field, as we would expect, but instead spans a region of very weak, and probably mixed field. Secondly, the ribbon in the south clearly becomes more regular – i.e., straighter – with time, while the underlying plage shows no change in its structuring. Thirdly, the ribbons do not move with the same speed along their length, and while in some locations the ribbon appears to move faster through lower flux regions (as one would expect – see later) this is not the case everywhere. For example in the southern ribbon at pixel number $\sim$ (65, 30) in Figure 4 (solar co-ordinates ($-20''$, $180''$) in Figures 1 and 2) the ribbons

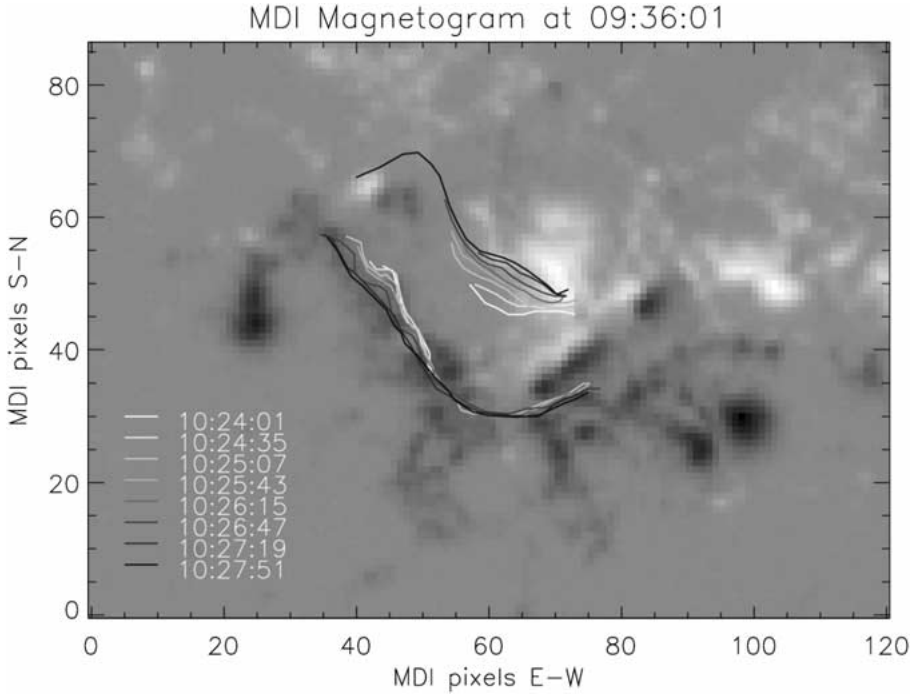

Figure 4. The positions of the outer edges of the EUV ribbons superimposed on the magnetic field. *White* indicates positive longitudinal field, and *black* negative.

do not move detectably, yet they are located again in apparently low field or even mixed-polarity field.

2.3. Evolution of the flare ribbons

In the standard model of flare evolution, a rising reconnection region results in ribbons (corresponding to the locations of chromospheric heating by beams or conduction) spreading apart through the photospheric magnetic field. The lighting-up of a footpoint thus indicates that a reconnection event has joined the footpoint to a counterpart on the other side of the neutral line, so that the movement of the ribbons indicates the magnetic flux which has been joined by reconnection. In this model, the expectation is that, since every positive source must be connected to a negative one, the total positive magnetic flux swept over by the ribbon on one side of the neutral line must equal that swept over by the ribbon on the other side. As a result of this, one would expect that ribbons moving through weak field regions would tend to move faster than ribbons moving through strong-field regions; Figures 4 and also 5 suggest that this is not everywhere the case. Ribbons move just as fast through high longitudinal field regions (i.e., 500–1000 G in the northern ribbon) as they do through lower field regions (i.e., −100 – −500 G in the south), and in

TABLE I

The magnetic fluxes, in units of 10^{20} Mx, measured between the positions of the northern and southern ribbons at the times indicated.

Time after 10 UT	25:07–28:58	25:07–26:15	26:15–27:19	27:19–28:58
South	-4.1 ± 0.5	-3.3 ± 0.4	-3.3 ± 0.3	-11.2 ± 0.5
North	1.2 ± 0.4	2.2 ± 0.6	2.4 ± 0.6	(1) 5.9 ± 1.6
				or (2) 6.2 ± 1.4

some of the lowest field regions they do not move at all. This may in fact help one decide which footpoints connect to which.

Our accurate overlay of ribbon positions on the magnetogram allows us to examine the flux traversed as a function of time in a quantitative way. We have chosen a number of time intervals from the beginning of the spreading of the flare ribbons, and, for both the northern and the southern ribbons, we total the magnetic flux contained in all of the pixels swept across by the ribbons. The one important thing to bear in mind when making this comparison is that the measurement returned by MDI is only of *line-of-sight* magnetic field strength. However, the region was very close to disk centre, so – if the photospheric field is predominantly vertical – the line-of-sight flux and the total flux should be approximately equal.

Table I shows the total flux in Maxwells traversed by the ribbons in the north and the south. Clearly the magnitudes of the two are not equal; the magnitude of the total flux traversed in the southern ribbon is on average 1.5 to 2 times more than in the northern ribbon. The two values (1) and (2) given correspond to the flux (1) without and (2) with the inclusion of the weak field region to the north, since it is not clear whether the ribbons are actually passing through this region, or just suddenly form.

It is worthwhile commenting on the manner in which the errors on these measurements are obtained. They are a combination of two factors; uncertainty in the alignment of the ribbons and the field (which we believe to be better than ± 1 MDI pixel in each direction) and also error in measuring the total flux, which is done by clicking on individual pixels and retrieving the field values from the MDI map structure. By offsetting the ribbon positions on the magnetogram by the ± 1 MDI pixel quoted above, and recalculating the total flux in each case we find that the error due to the first factor significantly outweighs that due to the second, particularly in the case of the northern ribbon which comes close to the strong field of a sunspot.

This mismatch between the flux in the northern ribbon and the flux in the southern ribbon may have a number of explanations:

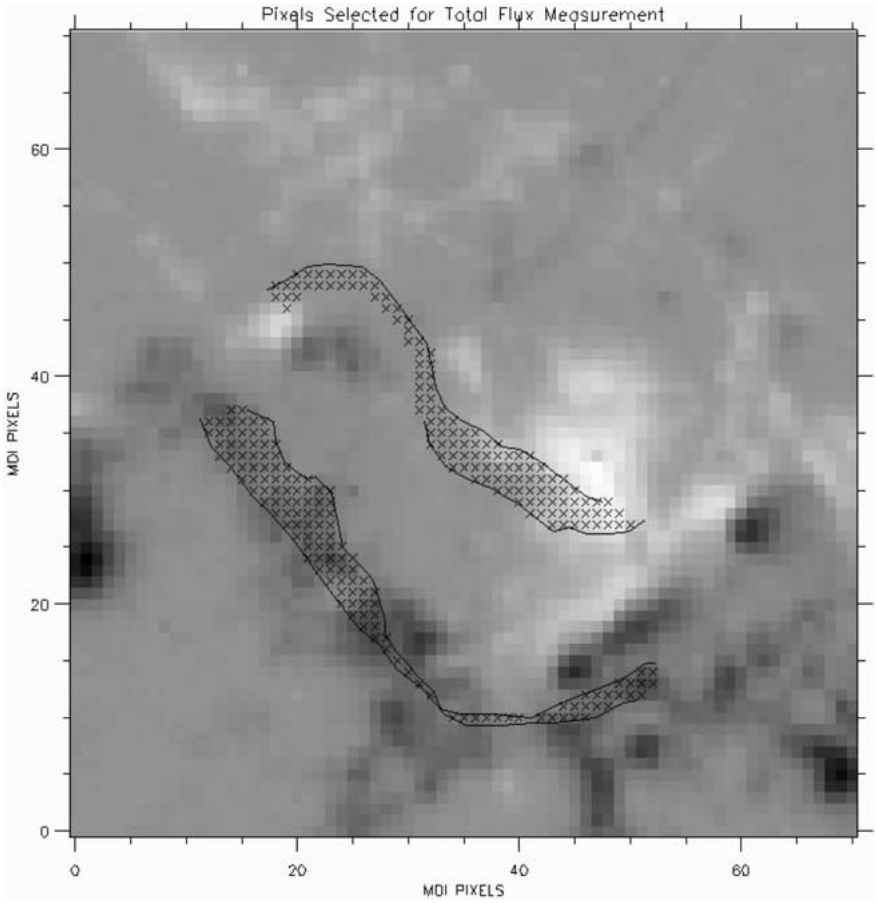

Figure 5. The pixels which are summed in the north and in the south to give the total flux measurement between 10:25:07 UT and 10:28:58 UT.

(a) The photospheric field in the northern ribbon may be inclined to the line-of-sight, so that the component measured by MDI is only ~ 0.5 of the total; i.e., the inclination angle is $\sim 60°$ to the LOS, or $\sim 44°$ to the local vertical. A high inclination angle in the strong positive field around the sunspot at $x = 0''$ (see Figure 10) would be sufficient to make up the deficit. This might in fact be expected if penumbral field, which is thought to be highly inclined to the vertical, is involved in the reconnection.

(b) Not all of the footpoints of magnetic field which has been reconnected are illuminated in 195 Å. This might be the case if the 195 Å emission is generated by bombardment, and fewer particles reach the footpoints in the positive-field side of the loop than the negative field regions. This can in principle be tested by comparing the HXR signatures from each field region, which we do in the next section.

(c) Not all field lines ending at the southern ribbon in fact reconnect during this event. This may be because (i) the southern ribbon is illuminated and moving as a result of an earlier reconnection event, by which the southern ribbon has conterpart positive field in other parts of the active region – e.g., the east, or (ii) if coronal reconnection is patchy then not all field ending in the ribbon has necessarily undergone reconnection, though with limited instrumental resolution it is not possible to see which footpoints are bright and which not.

(d) The field is structured on scales below that resolved by MDI and is weaker than the (spatially averaged) MDI measurements suggest, so that the total flux per pixel returned by MDI in the plage regions to the south of the neutral line is an over-estimate.

(e) The response of the MDI instrument to flux mixed on a small scale is such that in our region the positive flux is systematically underestimated, or the magnitude of the negative flux systematically overestimated.

Clearly, vector field measurements would enable us to determine whether (a) is true, while (b) can be tested in part by comparing HXR and EUV signatures for signs that they are generated by the same particle population. Regarding option (c)(ii), we have noted that the southern ribbon is already bright before the flare in the eastern part of the active region, suggesting that there are magnetic connections between the west and the east. This is particularly true of the parts of the ribbon around $(-20'', 180'')$. Post-flare loops do indicate possible connections between here and the western part of the active region. However, the flux traversed by this section of the southern ribbon is very small compared to that traversed by the rest of the moving ribbon, and not capable of explaining the disrepancy. Note however that if this portion of the southern ribbon is illuminated primarily as a result of the previous reconnection event, it would explain why there is apparently no ribbon motion here, despite the low field (see earlier in this section as well as Section 2.2).

Options (d) and (e) are related, both requiring that the flux in the plage field of the southern ribbon be concentrated into smaller fragments than the MDI images suggest; this is almost certainly the case. This may also apply to option (c)(ii). Using speckle interferometry on the photosphere, one observes the magnetic field to be concentrated into small-scale structures approximately 200 km wide (Keller, 1992) far below the resolution offered by MDI (with pixel size equivalent to 1500 km). The field measured by MDI is an average over the pixel, in which there are thus presumably areas of higher and lower field, as well as positive and negative elements. The MDI measured value is then a weighted average field. That this average may not be a good representation of the true average field present is suggested by the work of Berger *et al.* (2001) who find a lack of agreement between field measurements made with MDI and ASP magnetogram data, due to the lower resolution of MDI which blurs together small-scale field elements. In regions of mixed polarity, this results in the minority polarity being blurred with the majority polarity present, to give the impression of missing flux. If this effect – i.e., the degree of mixing of positive and negative field – were more pronounced

in the positive field region than in the negative regions, our discrepancy could be explained. However, there is no *a priori* reason to expect this, especially since the positive ribbons traverse less plage and more umbra than the negative ribbons.

Even within wholly positive or negative regions, the MDI magnetic observations may be weighted. The response of an instrument such as MDI involves factors such as (i) the diagnostic used (ii) the effect of photospheric stray light and scattering in the instrument. The diagnostic used is the difference between left and right-handed circularly polarized components of the Ni I 6768 Å absorption line, which is a measure of the Zeeman splitting and roughly proportional to the flux density. The diagnostic might thus be expected to be biased towards the higher field present. However, the effect of photospheric stray light tends to be to 'fill in' dark pores, leading to an understimate of fields present (Karel Schrijver, private communication). A more quantitative discussion is beyond the scope of this paper, but it is evident that it may not be possible to take MDI field measurements at face value.

Fragmentation of the field on a sub-MDI pixel scale is also necessary to explain the presence of northern flare ribbon in field which is apparently very weak field and without a dominant polarity. The sign of the field in the northern ribbon should be positive, so for a footpoint to form in this weak field there must in fact be significant positive flux concentrations present, the field-lines from which extend as far as the site of coronal reconnection. Ribbon locations even fall on MDI pixels which apparently have significant net negative LOS fluxes (see Figure 6); either they must also be sources of strong positive flux, or be one element of small bipoles which are excluded from the reconnection, or the photospheric field must be greatly inclined to the local vertical (i.e., more than 60°) so that the net measured longitudinal component is close to zero. This latter would be a completely different interpretation for weak, probably mixed-polarity field in this region.

3. Hard X-Ray Footpoints

By comparing with HXR emission, we are also able to consider the EUV generation mechanism, and in the process examine explanation (b) given above. As mentioned previously, illumination of the footpoints in EUV may be due to the direct bombardment of the atmosphere by particles, leading to either rapid heating, or to direct collisional 'impact' excitation of the transition region. This depends upon the density in the transition region that forms, as well as the energy and type of the bombarding particle. Alternatively, the footpoints may be illuminated because of atmospheric heating due to conduction from the heated loop to the lower atmosphere. A first discriminator between these methods will be to look at the time-profile of the EUV emission, and compare it with the time-profile of a signature which is known to be due to direct particle bombardment: HXR emission.

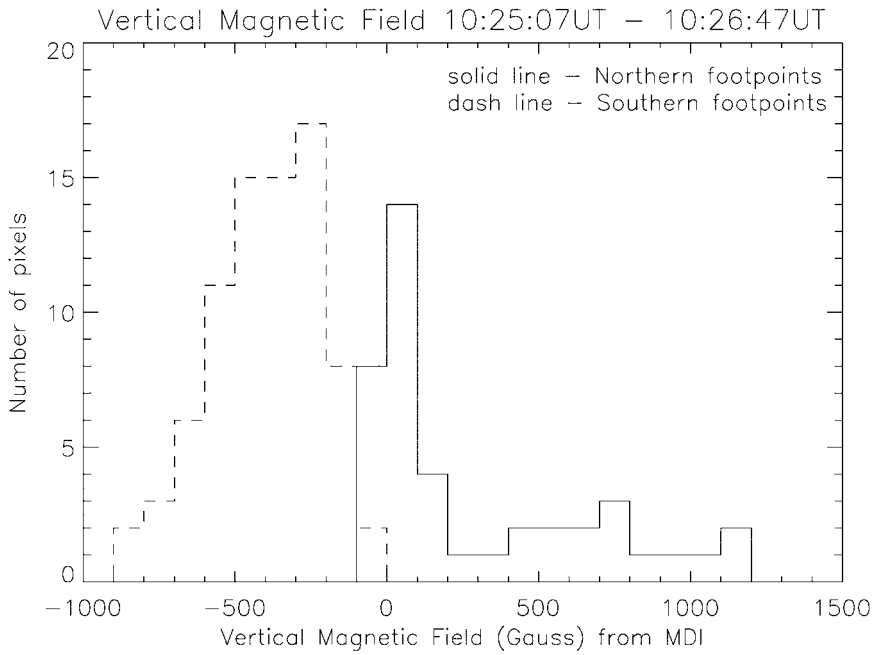

Figure 6. The histogram of field values in MDI pixels 'swept across' by the ribbons in the time interval indicated. Note, the error on MDI field values is ± 20 G – a small number of apparent footpoints in the northern (positive) ribbon have field values of −50 G and below.

Such studies have precedents in the pre-*Yohkoh* and TRACE era. The first reports of a time-correlation to within 1s between broad-band UV flux arriving at Earth during a flare and (spatially integrated) HXR flux were given upon by Kane and Donnelly (1971) and Kane, Frost, and Donnelly (1979) using data from the OGO and OSO satellites. A similar time correlation within some spectral lines was found with the UVSP and HXRBS instruments on board SMM (Woodgate *et al.*, 1983), but again no spatial information on the HXRs was available at the that time, and spatial resolution in UV was poor. We now have the possibility to compare HXRs and EUV with resolution in both space and time.

If the ribbons are produced as a result of direct bombardment by *electrons*, we would expect the EUV and HXR fluxes to vary in step, possibly with a slight lag if EUV is produced by heating, rather than by direct collisional excitation. If heating/excitation is by *protons* we need expect no such time correlation, though it may indeed be present (there is no *a priori* reason to expect that electrons, producing HXRs, and protons need be accelerated or precipitate with the same time-profile. However, we might yet expect in this case that the location of proton heating and the location of electron-generated HXRs is roughly the same, if they are produced in the same reconnection event.) If EUV emission results from conduction-driven atmospheric heating there need be no direct time-relationship between HXRs and the appearance of EUV footpoints, save that the heating would

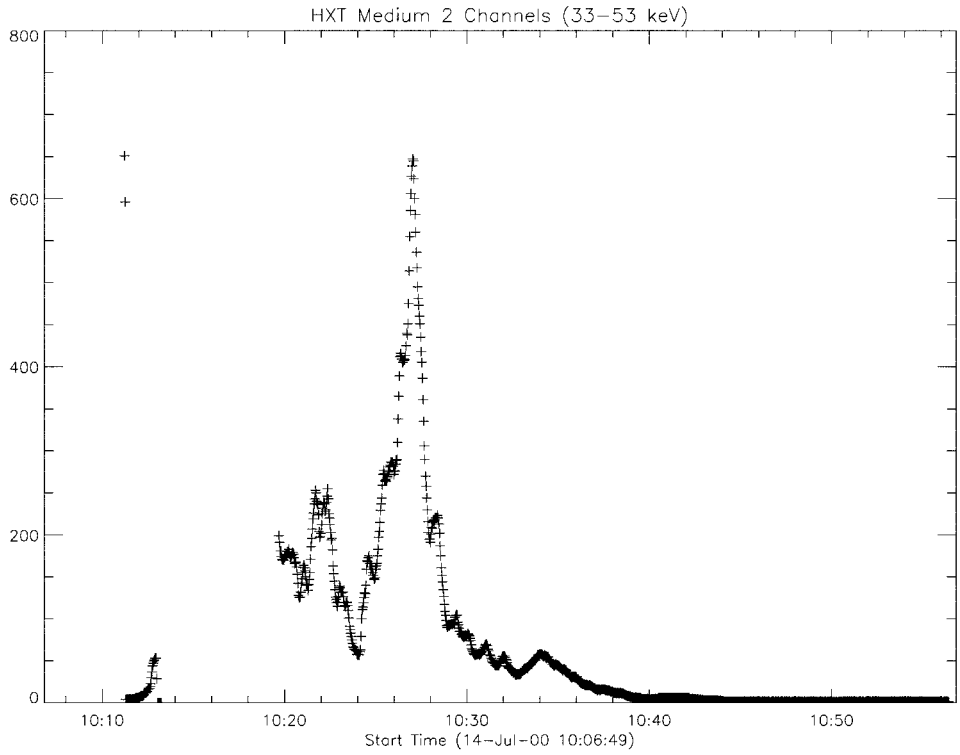

Figure 7. The light-curve in the *Yohkoh*/HXT 33–53 keV channel. The major peak is associated with the flare in the eastern part of the region.

lag a HXR spike. But the exact time relationship between the two would be determined by the loop heating following reconnection, and the hydrodynamic response of the chromosphere to it, which we will not consider in detail here.

3.1. Time evolution of EUV and hard X-ray intensity

The HXT M2 channel time profile is shown in Figure 7. The imaging capability of HXT also allows us to recover the positions of the principal HXR sources during this time; this is done using the Maximum Entropy reconstruction method. We co-align the reconstructed HXR sources made during the peak of the flare (at 10:27:00–10:27:20 UT) on the corresponding TRACE EUV image. Note that, due to the TRACE pointing offset, a blind coalignment based only on pointing information results in a clear misalignment of the brightest HXR and TRACE sources, with the HXT sources being located approximately 10″ to the south of the strongest TRACE sources. To correct for this, we assume that the HXR pointing is reliable (arguing that (a) the pointing of HXT relative to SXT is known to better than one SXT pixel, 2.5″ (Masuda, 1994), and that SXT pointing information is accurate) so that HXT and MDI images can be coaligned. The correction from MDI to TRACE

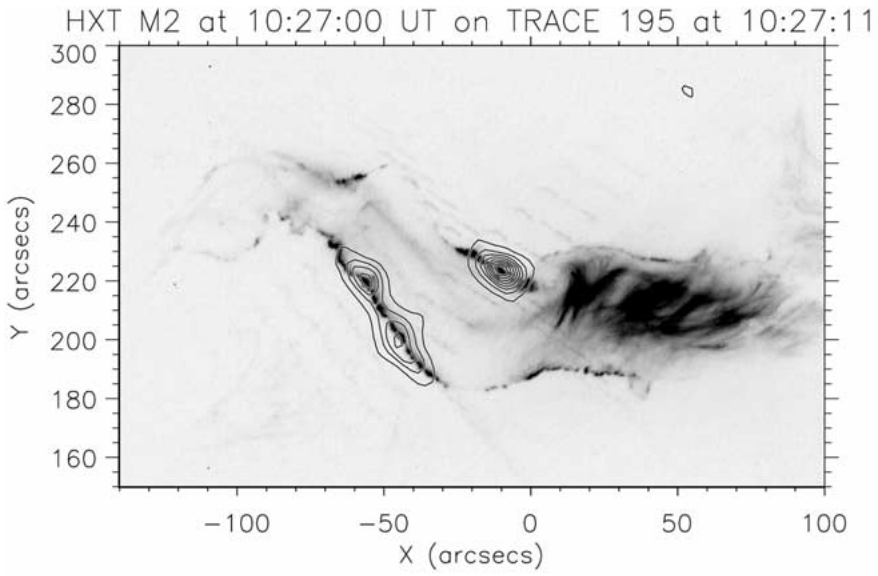

Figure 8. The position of the strongest HXT sources at the peak of the flare relative to the EUV sources.

images has been determined by cross-correlation as described previously; this is then applied and the HXT images can be overlaid on the TRACE images with a combined uncertainty in the positioning of $\sqrt{2.''5^2 + 2.''0^2} = 3.2''$. When this is done, we see that the strongest HXT M2 sources occur at the same locations as the strongest EUV sources, as evidenced by the diffraction patterns occurring in the EUV images (Figure 8).

We sum the counts per second in the (normalised) EUV images in small regions about the centroid of the HXR emission, and plot these as a function of time, along with the total counts per second in the M2 and also the HI channel. The results of this procedure appear in Figure 9. Although the TRACE time resolution is poor compared to that achieved by HXT ($\sim$4 s compared to 0.5. s for HXT), we can see that the curves map one another quite well; in particular the small peak at 10:26:10 UT is present in both sets of data. Unfortunately we do not have TRACE EUV data right at the peak of the HXR light-curve, which might allow us to determine whether the EUV peak is simultaneous with or delayed with respect to the HXR peak. With the current data, we can say only that the two peak within 20 s of each other.

The approximately linear relationships between the rates in the 195 Å channel and both the M2 and HI channels is interesting. This linearity certainly would be expected if the intensity of 195 Å emission were dependent on beam flux (as is the HXR emission), which is consistent with collisional impact excitation of the EUV radiation by the beam particles themselves. The EUV counts fall off rapidly after the peak, unlike what would perhaps be expected for a thermal generation

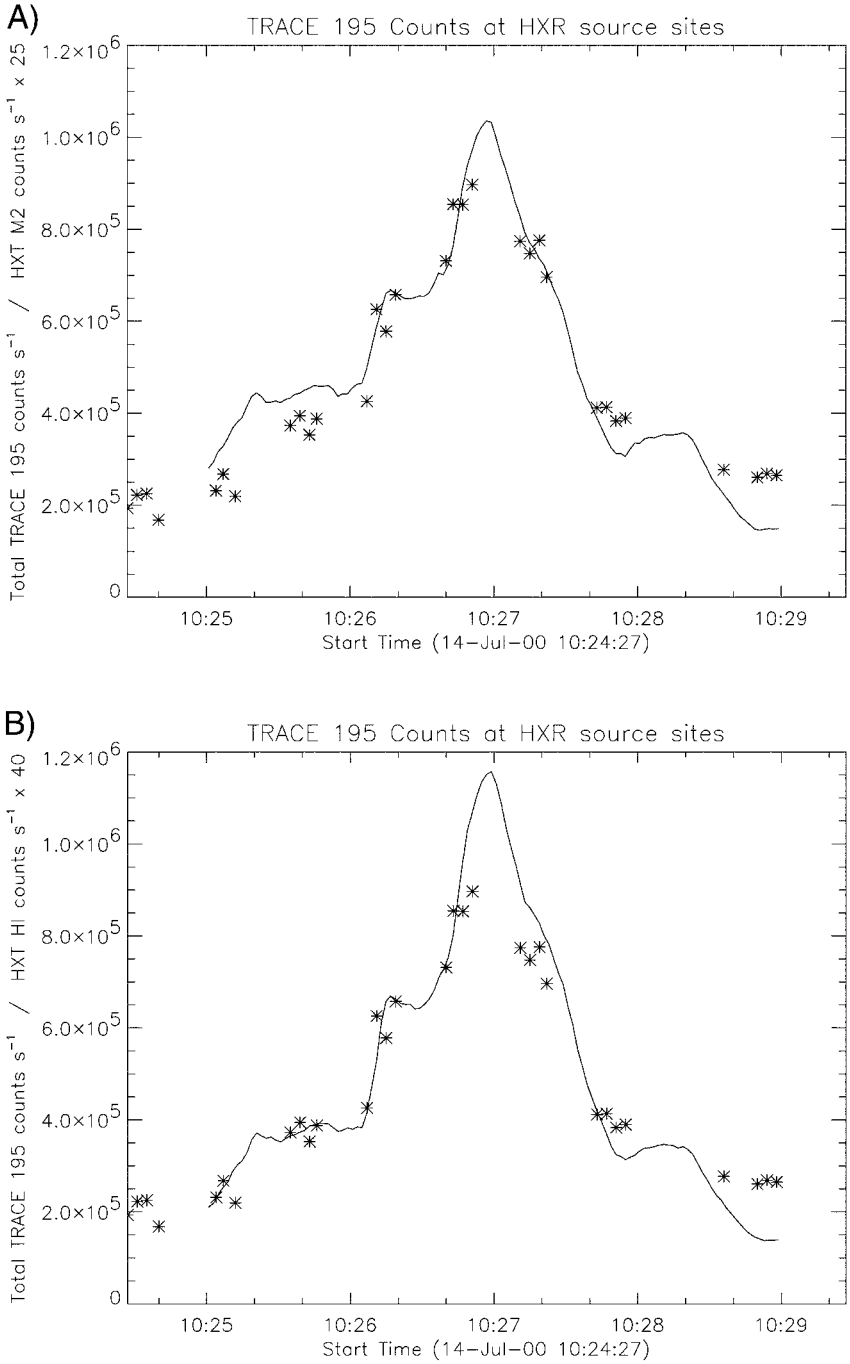

Figure 9. HXT scaled light curves (*solid lines*) on TRACE 195 Å source counts s^{-1}, measured at the locations of the HXT sources. The *upper plot* shows the M2 channel light curve, the *lower plot* shows the HI channel light curve. Note that the HXR light curves represent the total fluxes.

mechanism, which should have a more Neupert-like profile, following the time-integral of the HXRs. The exception to this would be if the EUV emitting material could conduct or radiate away its energy on timescales of less than 10 s or so. If energy loss were by radiation, this would imply a density in the radiating material of the order of $10^{11}-10^{12}$ cm^{-3}, depending on the abundance and temperature (this value for a temperature of a few 10^6 K). However, conduction downwards to the photosphere from a strongly-heated footpoint region, of small vertical extent, could also cause the source to vary on timescales of 10 s, for a more modest source density. This is evidently a matter for further study, and we go no further at this point than to say that the EUV profiles are consistent with direct impact excitation by beam particles, and possibly also with collisional heating, leading to increased thermal excitation, coupled with high radiative or conductive losses.

At a first glance, then, the EUV emission varies with the HXR signatures, and is consistent with either direct collisional excitation by electrons, or beam-generated heating, rather than thermal conduction from the loop above. Although the HXT data allows us to test this only at two or three points in the ribbons, we suggest that the EUV ribbons are generated by the same mechanism along their entire length.

The question which we hoped initially to address with this comparison was how the EUV ribbons are generated, and why the ribbons to the north appear to progress through less flux than those to the south, in the same length of time. The proposal was that for some reason we simply do not see all of the loop footpoints to the north, which, assuming ribbon generation by beam excitation, could be the case if electron precipitation were inhibited in the positive field region. This may be true – since part of the northern ribbon passes through strong positive field regions close to the positive sunspot, the stronger magnetic field could lead to mirroring, inhibiting precipitation in the north. We examine this possibility in the next section.

3.2. The relationship between HXR intensity and magnetic field strength

In the standard model the stronger HXR sources are expected to be in weaker field regions, since at the strong-field end of a loop, the higher degree of field convergence between coronal acceleration site and chromospheric precipitation site should produce a more efficient magnetic mirror. This inhibits precipitation and may bounce particles back towards the weak-field footpoint. This expected relationship was borne out by early HXT observations (Sakao, 1994).

In this event, the HXT source on the northern ribbon is always the dominant source between 10:26:40 UT and 10:28:20 UT. However it is located in a region of higher longitudinal field strength – typically 1000 G, compared to the sources in the south, which are located in regions of typically 500 G (Figure 10). This is contrary to what we expect in the magnetic-mirror interpretation. Furthermore, we have speculated that a possible reason for the mismatch in flux found in Section 2.2 would be for the measured line-of-sight field in the north, near the sunspot

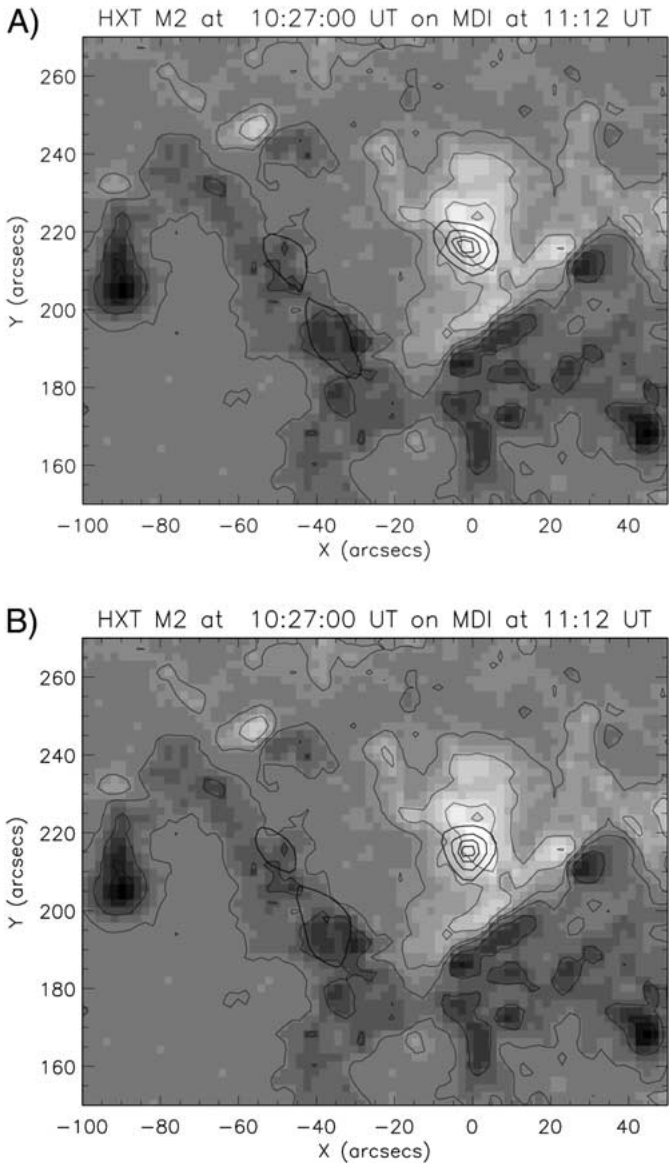

Figure 10. HXT source positions at HXR maximum overlaid on the MDI magnetogram. The HXT contours are at 25%, 50%, 75%, and 90% of the maximum, and the longitudinal magnetic field contours are at (−1000, −500, −100, 100, 500, 1000 G). M1 *top*; M2 *bottom*.

to be significantly less than the true field strength, meaning that the field at the location of the northern HXT footpoint could be yet stronger, further exacerbating the situation. So while the ribbons appear to be consistent with generation by electron precipitation, the HXR signatures do not vary in a way consistent with that expected for electron dynamics. This presents somewhat of a conundrum.

But again this neglects the possibility that the magnetic field is finely structured; the small bundle of field lines down which the HXR-generating electrons actually travel might end in an unresolved weak-field region.

4. Discussion and Conclusions

The major objective of this study has been to understand the magnetic environment of the flare ribbons in the context of their EUV and X-ray structure. We would like to understand the behavior of the flare ribbons, ideally well enough so that we can use the observations to learn something about the coronal dynamics involved in causing the flare. A more elaborate approach to this kind of study would involve the generation of coronal magnetic-field models. However, even without this problematic refinement, the flare we have studied has provided us with several interesting and some unexpected developments in spite of its extremely regular appearance. In a sense we are taking a first look at the reconnected magnetic flux that has actually provided the flare energy, in the standard model, and our flux measurement is a valuable input parameter to flare energy calculations.

We commented in Section 2 on two aspects of the ribbon development which we elaborate upon here. First of all, the ribbon to the south becomes more regular – straighter on both the large and small scale – as time goes on. There is nothing visible in the chromospheric field – no edge or gradient – to suggest why this should happen, therefore it must reflect some property of the coronal field distribution. In the rising reconnection model of the solar flare this suggests that the field lines closest to the initial reconnection site are not only more highly sheared than those farther away, but also possibly more tangled, or less able to rearrange themselves into a smooth mapping from coronal neighbours to photospheric neighbours.

Some parts of the ribbons developed parallel structures, which we have referred to as ‘bifurcation’. This is visible in the 1600 Å channel and to a lesser extent in the EUV channels. The outer (advancing) edge of the ribbon forms one element of a bifurcation. Our comparison with HXR data suggests that this advancing edge is bright as a result of electron precipitation, and dims again very soon after the site of precipitation has moved on. But once this happens, we are still left with a high-pressure, post-reconnection loop, which could lead to a ‘moss-like’ illumination of the underlying footpoints at the point when the balance of temperatures and pressures through the loop and underlying atmosphere is just right – so that lower atmosphere temperatures reach one million degrees or so. However, each loop of the arcade has a roughly isobaric nature, and in the standard model the pressure

would vary systematically with time and therefore ribbon location, and one might expect the brightness to do likewise. Why the bifurcation develops is a matter for modelling – possibly reflecting some bimodal effect of these varying parameters. It also might represent actual structural complications resulting from the redistribution of coronal overpressure. At present we cannot offer an explanation.

The possibility that not all of the magnetic field which ends in a flare ribbon undergoes reconnection is an interesting one, as it suggests that there can be a subset of the active-region field which does not participate in the reconnection event – the 'patchy reconnection' scenario discussed by Klimchuk (1997), possibly indirectly observed by McKenzie and Hudson (1999) via infalling blobs from discrete reconnection events. In some ways this is a more realistic scenario for what might happen in an arcade. There is no reason to suppose that reconnection – in a coronal field which is constantly being driven and tangled by photospheric motion – takes place in a uniform, homogeneous sheet or line above the arcade, but is likely to be fragmented along the length of the arcade, possibly by current-sheet instabilities, or possibly because the conditions which make reconnection possibly vary from place to place in the corona. How exactly the field might rearrange itself in such a scenario is puzzling; one would have to have have pre-reconnection, possibly sheared, field threading through post-reconnection un-sheared loops. However, the rearrangement and relaxation of just such a field may provide a further, gradual energy source for the arcade in its post-flare evolution.

Finally, we have found an obvious exception to the suggestion that the weaker-field footpoint should be the brighter one in hard X-rays. We know from microwave/HXR comparisons that mirroring and trapping do occur, so this discrepancy suggests further complication in the coronal dynamics.

Can the standard reconnection model incorporate the results presented here? For most of them, the level of observational detail is far beyond the competence of the MHD-based theories. In a global sense, this probably means that we have not found inconsistencies that may not eventually work themselves out. However, our first look at the 'reconnecting' magnetic fluxes – which should balance out precisely – is not reassuring. In addition this event reveals complexities in the relationship between the photospheric and coronal field (bifurcation, bipolar ribbon tracks, mirror-effect inconsistencies in the precipitation). The existence of these complexities hints at a more complicated coronal restructuring than the standard model requires.

Acknowledgements

NASA supported this work under contract NAS8-40801. *Yohkoh* is a mission of the Institute of Space and Astronautical Sciences (Japan), with participation from the U.S. (NASA) and U.K. (PPARC). L.F. thanks H. Potts and K. Schrijver for useful discussion, and PPARC for travel support to facilitate the collaboration.

References

Berger, T. E., De Pontieu, B., Fletcher, L., Schrijver, C. J., Tarbell, T. D., and Title, A. M.: 1999, *Solar Phys.* **190**, 409.
Berger, T. E., Lites, B., Martinez-Pillet, V. Tarbell, T., and Title, A.: 2001, *Solar Phys.* (in preparation).
Bruzek, A.: 1964, *Astrophys. J.* **140**, 746.
Czaykowska, A., Alexander, D., and De Pontieu, B.: 2001, *Astrophys. J.* **552**, 849.
Czaykowska, A., De Pontieu, B., Alexander, D., and Rank, G.: 1999, *Astrophys. J.* **521**, L75.
Domingo, V., Fleck, B., and Poland, A. I.: 1995, *Solar Phys.* **162**, 1.
Fletcher, L. and De Pontieu, B.: 1999, *Astrophys. J.* **520**, L135.
Kane, S. R. and Donnelly, R. F.: 1971, *Astrophys. J.* **164**, 151.
Kane, S. R., Frost, K. J., and Donnelly, R. F.: 1979, *Astrophys. J.* **234**, 669.
Keller C. U.: 1992, *Nature* **359**, 307.
Klimchuk, J.: 1997, in R. D. Bentley and J. Mariska (eds.), 'Magnetic Reconnection in the Solar Atmosphere' *ASP Conf. Proc.* **111**, 319.
Kopp, R. and Pneuman, G.: 19976, *Solar Phys.* **50**, 85.
Li, P., Emslie, A. G., and Mariska, J. T.: 1993, *Astrophys. J.* **471**, 313.
Martens, P. C. H., Kankelborg, C. C., and Berger, T. E.: 2000, *Astrophys. J.* **537**, 471.
Masuda, S.: 1994, Ph.D. Thesis, University of Tokyo.
Masuda, S., Kosugi, T., and Hudson, H. S.: 2001, *Solar Phys.*, this issue.
McKenzie, D. E. and Hudson, H. S.: 1999, *Astrophys. J.* **519**, L93.
Melrose, D. B.: 1997, *Astrophys. J.* **486**, 521.
Scherrer, P. H., Bogart, R. S., Bush, R. I., Hoeksema, J. T., Kosovichev, A. G. *et al.*: 1995, *Solar Phys.* **162**, 129.
Sakao, T.: 1994, Ph.D. Thesis, University of Tokyo.
Švestka, Z.: 1976, *Solar Flares*, Reidel, Dordrecht, Holland.
Woodgate, B. E., Shine, R. A., Poland, A. I., and Orwig, L. E.: 1983, *Astrophys. J.* **265**, 530.